Electrochemical Characterization of Halide Perovskites: Stability & Doping

*Sauraj Jha,[1] Mehedhi Hasan,[2] Nischal Khakurel,[2] Conor A. Ryan,[3] Reema McMullen,[3] Aditya Mishra,[1] Anton V. Malko,[3] Alexander A. Zakhidov,[2,4] and Jason D. Slinker[1,3]**

[1]Department of Materials Science and Engineering, The University of Texas at Dallas, 800 West Campbell Road, SCI 10, Richardson, Texas 75080-3021, United States

[2]Materials Science, Engineering, and Commercialization, Texas State University, San Marcos, Texas 78666, United States

[3]Department of Physics, The University of Texas at Dallas, 800 West Campbell Road, Richardson, Texas 75080-3021, United States

[4]Department of Physics, Texas State University, San Marcos, Texas 78666, United States

AUTHOR INFORMATION

Corresponding Author

*slinker@utdallas.edu

Keywords

cyclic voltammetry, methylammonium lead iodide, electrochemistry, degradation, hydrofluoroether

Abstract

As halide perovskite materials have emerged at the forefront of optoelectronics development, there is an ongoing need to understand their underlying physics and control their emergent properties. Electrochemistry shows promise to both access fundamental parameters of perovskites and to enhance their performance through doping. However, halide perovskites pose a significant challenge to solution-based electrochemistry, as both aqueous solutions and organic solvents are often destructive to thin films of these materials. This work provides a perspective of recent approaches to electrochemical measurements and modifications of halide perovskites with a specific focus on stability and doping. We also report the electrochemistry of methylammonium lead iodide ($MAPbI_3$) thin films relevant for solar applications with a solvent toolkit based on hydrofluoroethers. Both oxidation and reduction peaks are revealed from electrochemical characterization exhibiting the characteristic HOMO/LUMO levels and additional features. This electrochemical driving is found to have little impact on the photoluminescence or underlying morphology of the thin films. Finally, electrochemical lithium salt doping with this solvent toolkit enhanced the conductivity of a thin film device by nearly two orders of magnitude, demonstrating the utility of this approach for optoelectronic applications.

1. Introduction

1.1 Overview

Halide perovskites are under intense study for their beneficial electronic and optoelectronic properties, including high carrier mobility, tunable bandgap, charge storage capacity, and high power efficiency for solar conversion[1-2] and electroluminescence.[3-4] These favorable transport[5-7] and optical[8-11] properties are tied to their underlying electronic states that can be modulated by choosing cations, halide anions, dopant molecules, and structure. Ultimately, rational optimization of halide perovskites necessitates understanding the impact of composition and morphology on energy band levels.

Electrochemistry offers a powerful means of accessing the fundamental energetics of halide perovskites. Voltammetry, amperometry, and impedance spectroscopy can be leveraged to reveal frontier and excited state orbitals, defect and dopant states, densities of states, electron and hole transfer rates, conductivities, dielectric constants, and equivalent circuits. Another benefit of perovskite electrochemistry is doping. There are fruitful synthesis-based approaches to doping perovskite materials, such as through nonstoichiometric combinations of perovskite precursors or the inclusion of trivalent ions during synthesis.[12-17] Electrochemical approaches offer unique benefits over traditional synthetic approaches.[18-24] Voltage and time may be controlled precisely to access specific chemical transitions and smoothly vary resulting modifications. Furthermore, measuring the voltammograms through the doping process enables rapid feedback of evolving doping processes. Electrochemical modification of perovskites also decouples crystal formation and doping, as doping can be performed after forming the thin film or crystal sample.

However, it is challenging to perform electrochemistry on thin films of halide perovskites, as both aqueous and organic solvents can disrupt the structure or dissolve the film. Nonetheless, approaches are emerging to perform electrochemistry with minimal damage to the perovskite. This work provides a perspective of progress in perovskite electrochemistry with a specific focus on stability and doping. Subsequently, we disclose our recent experimental results with a hydrofluoroether (HFE) solvent toolkit. We perform cyclic voltammetry (CV) of a methylammonium lead iodide ($MAPbI_3$) thin film in this HFE electrolyte solution, identifying characteristic oxidation and reduction features. Subsequently, the impact

of electrochemical oxidation and reduction on photoluminescence (PL) and morphology (SEM) are explored. Finally, the HFE solvent toolkit is leveraged to dope a $MAPbI_3$ thin film electrochemically.

1.2 Perspective of Progress

Jiang et al. performed electrochemical measurements and doping of a composite perovskite film.[18] The film, composed of $CsPbBr_3$, conductive carbon black, and polyvinylidene fluoride (PVDF), was prepared on a copper foil and utilized as the working electrode for CV. The electrolyte was a mixture of 1.0 M bis(trifluoromethane) sulfonimide lithium salt (LiTFSI) in 1,3 dioxolane/dimethoxyethane in a 1:1 volume ratio. The resulting CV is shown in Figure 1 for a scan from 2.8 V to 0.05 V against a Li/Li^+ reference. A clear and highly reversible cathodic peak was visible at 0.93 V, consistent with electrochemical reduction. Scanning electron microscopy (SEM) and X-ray diffraction (XRD) studies showed that the $CsPbBr_3$ crystals evolved a rougher surface morphology from electrochemical doping but retained the same overall orthorhombic crystal structure. Reversible electrochromic behavior, from yellow to black, was observed from the lithium doping process. Other lithium salts, such as $LiClO_4$ and $LiCF_3SO_3$, were reported as compatible, as were other perovskites, such as $CsPbBr_2Cl$, $CH_3NH_3PbCl_3$, and $CsPb(SCN)_2Br$. Thus, a straightforward electrochemical approach was established, enabling the measure and doping of perovskites with a minor impact on the composite film morphology. In follow-up work,[19] members of this group demonstrated that this lithium doping was shown to lead to diamagnetic behavior in $CsPbBr_3$ crystals, with a critical temperature of 7.17 K. A 15 nm blueshift in the PL upon doping was attributed to the Burstein—Moss effect, and a fourfold enhancement in photocurrent from lithium doping was also observed.

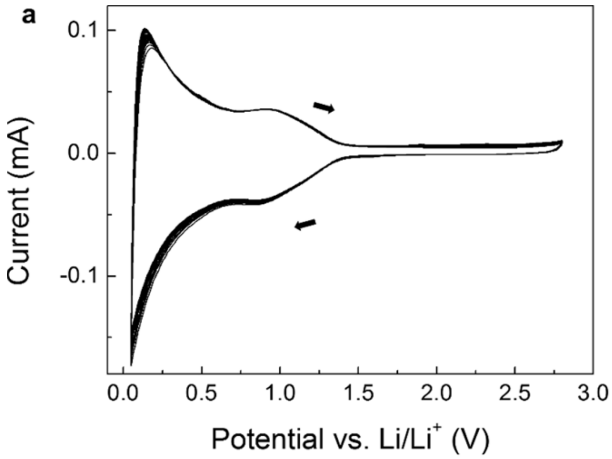

Figure 1. CV (10 mV/s scan rate) of a $CsPbBr_3$ composite electrode vs Li/Li^+. The arrows indicate the scan direction. Reproduced with permission from Ref. 18. 2017 American Chemical Society.

Vicente and Garcia-Belmonte carefully studied the uptake and release process of lithium doping in a methylammonium lead bromide perovskite matrix.[21] Perovskite anodes were formed by mixing $CH_3NH_3PbBr_3$, carbon black, and PVDF, and coating the slurry on copper foil. They performed electrochemical doping and measurements with an electrolyte of 1 M of hexafluorophosphate lithium salt dissolved in ethylene carbonate, ethyl-methyl carbonate, and dimethyl carbonate at a 1:1:1 volume ratio. Their CV results of lithium doping are shown in Figure 2. CV revealed redox peaks related to Li^+ insertion at 0.49 and 0.27 V vs. Li/Li^+, and Li^+ extraction at 0.65 and 0.75 V. The redox response was shown to be highly reversible over four cycles. Furthermore, electrochemical cycling produced a ~0.3 eV increase in the binding energies of the characteristic Pb 4f and Br 3p levels as measured from XPS, and this shift reversed on delithiation. Likewise, the lattice constant as measured by XRD showed a slight increase with lithium doping. Thus, it was argued that lithium doping occurred by topotactic insertion into the perovskite with minimal impact on the overall perovskite structure.

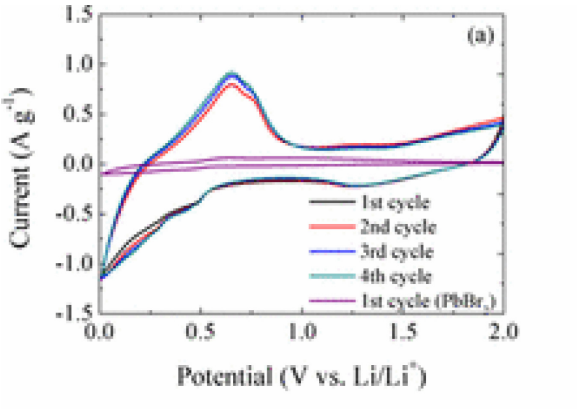

Figure 2. CV voltammograms of $CH_3NH_3PbBr_3$ electrodes for the first four cycles compared to a $PbBr_2$ electrode. Reproduced with permission from Ref. 21. 2017 American Chemical Society.

Dawson et al. utilized a combination of density functional theory (DFT) and electrochemistry coupled with diffraction to understand the fundamentals behind lithium uptake reactions and perovskite electrochemical performance.[20] DFT was performed with the ab initio code VASP with the PBEsol exchange-correlation functional on $CH_3NH_3PbX_3$ perovskites, where X is a halide. Lithium intercalation voltages were found to be highly dependent on the specific Li concentration, perovskite halide, and perovskite structure, ranging between 0 to 1.4 V. The electrochemical discharge profile of $CH_3NH_3PbBr_3$ revealed a specific capacity for discharge of 134.3 mA h g^{-1}, and the charge passed correlated with 2.4 Li^+ ions per perovskite molecule, well beyond the intercalative limit. Powder x-ray diffraction studies showed evidence for the formation of Pb-rich byproducts. It was ultimately postulated that $LiPbX_2$, LiX, Pb, and CH_3NH_3X products were formed. The reaction energies for the degradation products for each halide perovskite were calculated, and the LiX + Pb + CH_3NH_3X reactions were found to be energetically favorable to the desired intercalation product for all halides and substantially halide-dependent. This study helped explain the relative performance of $CH_3NH_3PbX_3$ anodes by clarifying atomic-level mechanisms.

In order to establish the bounds of electrochemical stability of inorganic $CsPbBr_3$ and hybrid organic-inorganic methylammonium lead iodide ($MAPbI_3$) perovskites, Samu et al. performed spectroelectrochemistry coupled with microscopic characterization.[24] Perovskite films were immobilized on TiO_2-coated fluorine-doped tin oxide (FTO), and dichloromethane with tetrabutylammonium hexafluoride was used as the electrolyte. For $CsPbBr_3$, a sharp oxidation peak near 0.8 V increasing 518 nm absorption and a broad peak beginning near 1.3 V decreasing 518 nm absorption were observed versus an Ag/AgCl reference. A single reductive peak was seen near −1.4 V vs. Ag/AgCl that decreased 518 nm absorption. XPS and XRD analysis revealed that Pb and PbO were formed during the reductive sweep, whereas $CsPF_6$ was formed on oxidation. For $MAPbI_3$, spectroelectrochemistry revealed two oxidation peaks and one reduction step at +0.8 V, +1.1 V, and −0.75 V vs. Ag/AgCl, respectively, while a cathodic shoulder was seen at −0.95 V. All of these peaks decreased the characteristic absorbance at 470 nm. Films were considerably less stable, and similar oxidation and reduction byproducts were proposed for $MAPbI_3$ and $CsPbBr_3$. Ultimately, electrochemical windows of −1.0 to +0.6 V vs. Ag/AgCl for $CsPbBr_3$ and −0.65 to +0.55 V vs. Ag/AgCl for $MAPbI_3$ were concluded as best practice for the electrolytes used.

Mulder et al. coupled spectroelectrochemistry and electrochemical transistor measurements to dope $CsPbBr_3$ nanocrystals electrochemically.[22] The perovskite nanocrystals were deposited on thiol-terminated self-assembled monolayers on ITO and subsequently crosslinked. They were electrochemically interrogated in an electrolyte solution of 0.1 M tetrabutylammonium hexafluorophosphate ($TBAPF_6$) in propylene carbonate. The cell used a silver wire pseudo reference electrode and a platinum sheet counter electrode. Concerning electrochemical stability, potentials more negative than −0.6 V versus NHE induced significant irreversible optical changes to the films, while potentials more positive than +0.9 V versus NHE

induced irreversible bleaching of the films and quenching of the PL indicative of degradation. However, the positive potentials simultaneously produced a reversible increase in conductivity as measured by electrochemical transistor operation, indicating reversible p-doping of the nanocrystals. In support of these stability observations, DFT calculations showed that while injected holes remained delocalized in the valence band, injected electrons localized on Pb^{2+}. The standard reduction potentials of possible degradation reactions were estimated, with reduction of Pb^{2+} to Pb^{0} shown to be particularly accessible, and oxidation of Br^{-} just beyond the valence band.

1.3 A Solvent Toolkit for Perovskite Electrochemistry

Our electrochemical characterization and doping approach utilizes a modular solvent toolkit based on hydrofluoroethers (HFEs). These highly fluorinated fluids offer alternative performance to typical polar and nonpolar solvents, behaving like an "orthogonal solvent".[25] HFEs can alternatively process organic, inorganic, and hybrid electronic materials without degradation.[23, 25-27] We applied this solvent toolkit approach to characterize methylammonium lead iodide perovskite films electrochemically.[23] A 3% v/v solution of diethyl carbonate in HFE 7100 hydrofluoroether was used to dissolve 0.1 M LiTFSI for the electrolyte. CV revealed an anodic peak at 4.96 V vs. Li/Li^{+} and a cathodic peak at 4.65 V vs. Li/Li^{+}. A highest occupied molecular orbital energy level of −5.64 eV was found in agreement with literature reports. Moreover, solution processing with this solvent toolkit did not alter the photovoltaic performance of solar devices. Solar cells with buckminsterfullerene (C_{60}) and bathocuproine (BCP) transport and blocking layers were fabricated, and the power conversion efficiency (13.5%) was unaffected by 5 min treatment in the HFE mixture followed by rinsing to remove excess salt. Thus, the HFE solvent toolkit was

demonstrated as a promising nondestructive approach for characterizing and processing perovskite thin films specifically prepared for solar applications.

2. Material and methods

2.1 Perovskite Ink Solution Preparation

A 1:1:1 molar ratio, 1 M perovskite ink of lead iodide, methylammonium acetate, and methylammonium iodide was prepared as described previously.[28] Lead (II) iodide (Tokyo Chemical Industry, 99.99%) was dissolved in anhydrous N, N-dimethylformamide (Sigma-Aldrich, 99.8%) by stirring at 700 rpm at 70 °C for 30 mins followed by room-temperature addition and stirring of methylammonium iodide (Lumtec, 99.5%) and methylammonium acetate (Greatcell Solar Materials), respectively. The solution was stirred for one hour and was filtered using a nylon syringe filter (0.22 μm pore size, Aireka Cells) immediately before spin coating.

2.2 Device Fabrication

Prepatterned ITO/glass substrates (150 nm, ~20 Ω sq^{-1}) were purchased from Thin Film Devices, Inc. These slides were cleaned in a sequence of non-ionic detergent wash, water bath sonication, and UV ozone treatment. The filtered perovskite ink was dispensed at the center of the substrate and was spin cast (SCS Spincoat G3P-8) with a 5 s ramp time and 60 s spin duration followed by 100 °C annealing for 10 mins (04644 Digital Hotplate, Cole Palmer).

2.3 Electrochemical Testing

A three-electrode configuration was used for electrochemical measurements with a non-aqueous Ag/AgCl reference electrode (eDAQ, Inc.) and a platinum wire as a counter electrode. The

electrolyte was prepared by dissolving 0.1 M $LiPF_6$ (battery grade, ≥ 99.99% trace metals basis) in diethyl carbonate (DEC, anhydrous, ≥ 99%, Sigma-Aldrich). The mixture was then added to a HFE solvent (3M Novec 7500, 3-Ethoxyperfluoro(2-methylhexane)) that had been previously degassed by bubbling argon gas for 60 mins. Electrochemical measurements were performed on a vibration isolation table using a CHI750D Electrochemical Analyzer and a CHI684 multiplexer under argon atmosphere. An optimum sweep rate for CV was found to be 10 mV s^{-1}.

2.4 Electrochemical Doping and Electrical Conductivity Measurement

$MAPbI_3$ was deposited by spin coating on an ITO (90nm) coated glass substrate using a 1:1:1 molar ratio of 1 M solutions of lead iodide, methylammonium acetate, and methylammonium iodide solution as described.[28] Deposition was performed in a N_2-filled glovebox (0% relative humidity), followed by annealing at 100° C for 5 min in a 45% relative humidity environment. After annealing, samples were divided into two pieces for electrochemical doping and stored in a N_2 glovebox. Electrochemical doping was performed inside the argon glovebox as described in Section 3.3. A 50 nm thick film of Au was deposited using a Trovato 300C thermal evaporator (located inside the N_2 glovebox) on both the undoped reference samples and doped samples in a single session to ensure identical film thickness and process parameters. I-V measurements of these $MAPbI_3$ films sandwiched between ITO and Au (as shown in the inset of Figure 5) were performed in a N_2 glove box with a Keithley 2400 sourcemeter.

2.5 PL Spectra

PL spectra measurements were performed in a microscope-based photoluminescence (μ PL) system. The $MAPbI_3$ thin films were excited by 400 nm laser pulses from a pulsepicked, frequency

doubled femtosecond Ti:sapphire oscillator (Coherent MIRA) at a power of 5 μW. A laser beam was focused on the sample by a Leica air microscope objective (32×, 0.6 NA). The PL signal was emitted into the collection aperture of the lens and sent to the system. The collected emission was passed through a spectrometer and directed to a CCD camera for a spectral analysis.

2.6 Scanning Electron Microscopy (SEM)

Secondary electron SEM images were taken with a Zeiss Supra-40 SEM using an in-lens detector at an accelerating voltage of 10kV.

3. Results and Discussion

3.1 *CV of $MAPbI_3$ in HFE*

a)

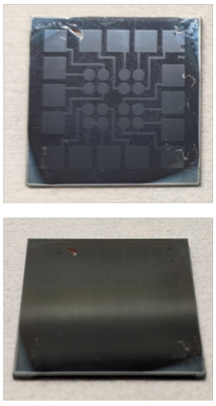

b)

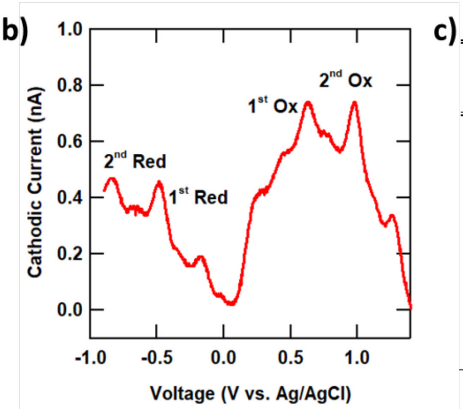

c)

Peak	Potential [vs Ag/AgCl]	Energy [eV]
2nd Red	−0.83	−3.85
1st Red	−0.48	−4.20
1st Ox	0.63	−5.31
2nd Ox	0.98	−5.66

Figure 3. (a) Images of $MAPbI_3$ thin films on ITO/glass substrates. (The film was removed from the square outer contact pads before measurement.) (b) CV (10 mV/s) of a $MAPbI_3$ thin film in HFE electrolyte. This spectrum has been processed with a linear baseline correction. (c) Summary of the first and second major oxidative and reductive peaks obtained from the CV of Figure 3b.

Thin films of $MAPbI_3$ were prepared in the characteristic black form[29] associated with solar cell applications, as shown in Figure 3a. We recorded the broad CV signal associated with

electrochemistry from a $MAPbI_3$ thin film using a HFE solvent toolkit electrolyte solution, as shown in Figure 3b. 0.1 M $LiPF_6$ in HFE7500:DEC (95:5 v/v) was used for the electrolyte, and CVs were recorded at a 10 mV/s scan rate. Four prominent peaks are apparent, with additional smaller peaks and shoulders as well. The potentials for each of the four dominant peaks are presented. These peaks show good agreement with those previously reported in literature.[23, 24] The second oxidation peak (at −5.64 eV) is in excellent agreement with our previous report[23] of the highest occupied molecular orbital (HOMO) peak for $MAPbI_3$ (at −5.66 eV) and likewise in good agreement with ultraviolet and x-ray photoelectron spectroscopy measurements.[30-32] Furthermore, although not discussed, close inspection of the electrochemistry prior work[23] reveals a small peak in the vicinity of the second reduction peak shown here in Figure 3 (−3.85 eV), which is attributed to the LUMO. Concerning other dedicated electrochemistry reports, our measurements agree well with the report of Samu et al. for all four peaks shown, within 0.2 eV for all peaks and within 0.04 eV for second oxidation and reduction features.[24] Three of these peaks bear a strong correlation with the $CsPbBr_3$ peaks reported by Mulder et al.:[22] the first reduction peak at -4.20 eV, the first oxidation at −5.31 eV, and the second oxidation peak already noted. The first reduction peak has been attributed to reduction of the Pb^{2+} to Pb^0, while the oxidation peak has been credited to the oxidation of the halide anion. The additional peaks may be characteristic of the microstructure features associated with the black films,[29] particularly those arising from the diammonium alpha phase. Thus, this solvent toolkit supports measure of the oxidative and reductive sweeps, identification of characteristic peaks, and observation of subtle details of the film.

3.2 PL and SEM Stability Characterization

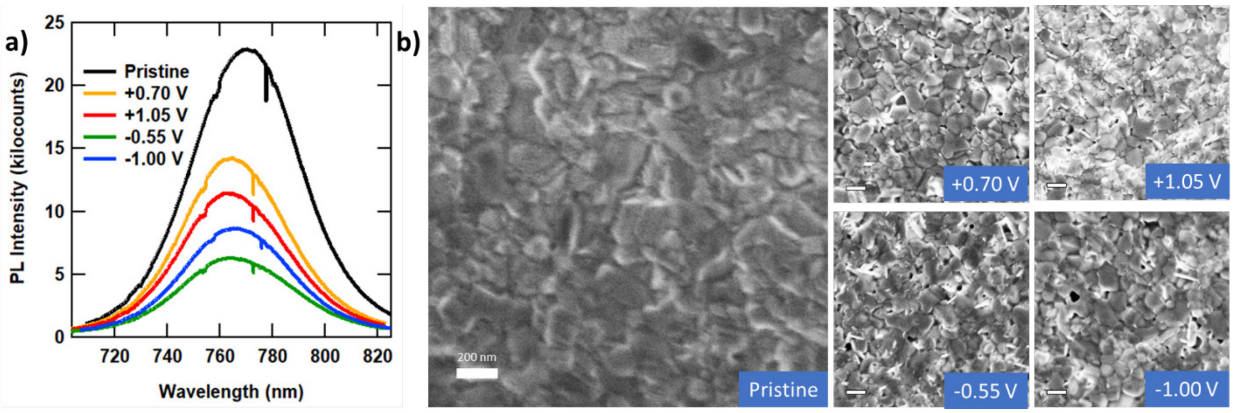

Figure 4. (a) PL of thin $MAPbI_3$ films before and after voltage sweeping to various electrochemical potentials versus Ag/AgCl. (b) Scanning electron microscopy images of thin $MAPbI_3$ films before and after voltage sweeping to various electrochemical potentials versus Ag/AgCl. The scale bars are 200 nm.

Subsequently, we characterized the impact of electrochemical characterization with the HFE solvent toolkit on the optical and morphological properties of the $MAPbI_3$ thin films. We investigated the changes from sweeping the voltage from 0 V versus a Ag/AgCl reference to each of the four major peaks (two oxidative and two reductive) noted from electrochemistry and compared to the properties of a pristine film that had not been electrochemically driven. In Figure 4a, the PL spectra of $MAPbI_3$ films before and after electrochemical testing are shown. The excitation wavelength was 400 nm. The pristine film shows a single peak of roughly Gaussian shape centered near 770 nm, with a full width at half maximum (FWHM) of 29 nm. Electrochemical testing induced very little change, with a slight 4-5 nm blueshift consistent with lithium ion uptake[18, 19, 33] and little change to the FWHM. Thus, electrochemical sweeping had minimal impact on the emission properties.

In Figure 4b, we investigated electrochemically-induced changes to the morphology of the $MAPbI_3$ films. A characteristic pattern with ~100-300 nm crystal domains is evident in the pristine

film. This overall structure is preserved in the films that were measured electrochemically to various voltages in the solvent toolkit. Some additional image contrast is present in the electrochemically-driven films, which is likely due to a combination of charging, salt deposits, and possible precipitates from the electrochemical driving. The most notable contrast changes are seen in the film biased to 1.05 V versus Ag/AgCl. Regardless, the SEM images reveal an overall preservation of the underlying structure of the perovskite film.

3.3 Electrochemical Doping

Finally, we demonstrate electrochemical doping of a $MAPbI_3$ film with our solvent toolkit. A 50 nm thick $MAPbI_3$ film on ITO was used as a working electrode with Li metal wire and Li metal mesh as the reference and counter electrodes, respectively. A constant current at 0.2 $\mu A/cm^2$ was applied for 300 s in a three-electrode scheme in 0.1 M LiTFSI in HFE7100:DEC (97:3 v/v) electrolyte. After doping the 50 nm $MAPbI_3$ film, the sample was removed from the electrolyte, rinsed in clean HFE7100 for 30 seconds, and dried with a gentle argon flow. Subsequently, a top Au metal electrode was deposited, and the current-voltage properties of the resulting device were measured and compared with that of the reference sample without doping (Figure 5). The reference device has a Shottky diode rectifying behavior, while the charged sample showed Ohmic behavior with absolute current values approximately two orders of magnitude higher than that of the reference device. Thus, electrochemical doping with lithium salts from a solvent toolkit can significantly enhance device conductivity, beneficial for optoelectronic applications.

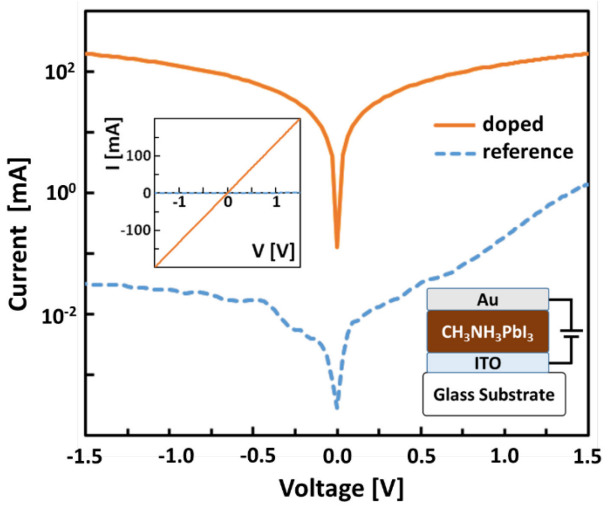

Figure 5. Current-voltage characteristics of doped and reference $MAPbI_3$ films. The inset shows the device stack and a linear plot of the current.

4. Conclusion

Electrochemistry of perovskites has shown promise for revealing key energy levels of the system, identifying failure modes, and enabling doping for enhanced electronic and optoelectronic applications. Here, with a HFE solvent toolkit, we identify the first four prominent electrochemistry peaks of $MAPbI_3$, particularly the peaks associated with the HOMO and LUMO. This electrochemistry is shown to have minimal impact on the PL and morphology of $MAPbI_3$ thin films. Electrochemical doping with the HFE electrolyte and a lithium salt increased the conductivity of a $MAPbI_3$ device by nearly two orders of magnitude. Thus, electrochemistry with a HFE solvent toolkit enables the stable measure and doping of perovskites for enhanced understanding and operation of electronics and optoelectronics.

Declaration of Competing Interests

The authors declare that they have no conflict of interest.

Acknowledgments

This work was supported by the National Science Foundation (ECCS 1906505 & ECCS 1906492).

Data availability

The data has been archived on Box.net and is available from the corresponding author.

References

1. Kim, J. Y.; Lee, J.-W.; Jung, H. S.; Shin, H.; Park, N.-G., High-Efficiency Perovskite Solar Cells. *Chem. Rev.* **2020,** *120* (15), 7867-7918.
2. Jeong, J.; Kim, M.; Seo, J.; Lu, H.; Ahlawat, P.; Mishra, A.; Yang, Y.; Hope, M. A.; Eickemeyer, F. T.; Kim, M.; Yoon, Y. J.; Choi, I. W.; Darwich, B. P.; Choi, S. J.; Jo, Y.; Lee, J. H.; Walker, B.; Zakeeruddin, S. M.; Emsley, L.; Rothlisberger, U.; Hagfeldt, A.; Kim, D. S.; Grätzel, M.; Kim, J. Y., Pseudo-halide anion engineering for α-$FAPbI_3$ perovskite solar cells. *Nature* **2021,** *592* (7854), 381-385.
3. Kim, Y.-H.; Kim, S.; Kakekhani, A.; Park, J.; Park, J.; Lee, Y.-H.; Xu, H.; Nagane, S.; Wexler, R. B.; Kim, D.-H.; Jo, S. H.; Martínez-Sarti, L.; Tan, P.; Sadhanala, A.; Park, G.-S.; Kim, Y.-W.; Hu, B.; Bolink, H. J.; Yoo, S.; Friend, R. H.; Rappe, A. M.; Lee, T.-W., Comprehensive defect suppression in perovskite nanocrystals for high-efficiency light-emitting diodes. *Nat. Photonics* **2021,** *15* (2), 148-155.
4. Ma, D.; Lin, K.; Dong, Y.; Choubisa, H.; Proppe, A. H.; Wu, D.; Wang, Y.-K.; Chen, B.; Li, P.; Fan, J. Z.; Yuan, F.; Johnston, A.; Liu, Y.; Kang, Y.; Lu, Z.-H.; Wei, Z.; Sargent, E. H., Distribution control enables efficient reduced-dimensional perovskite LEDs. *Nature* **2021,** *599* (7886), 594-598.
5. Zhao, D. W.; Chen, C.; Wang, C. L.; Junda, M. M.; Song, Z. N.; Grice, C. R.; Yu, Y.; Li, C. W.; Subedi, B.; Podraza, N. J.; Zhao, X. Z.; Fang, G. J.; Xiong, R. G.; Zhu, K.; Yan, Y. F., Efficient two-terminal all-perovskite tandem solar cells enabled by high-quality low-bandgap absorber layers. *Nat. Energy* **2018,** *3* (12), 1093-1100.
6. Wehrenfennig, C.; Eperon, G. E.; Johnston, M. B.; Snaith, H. J.; Herz, L. M., High Charge Carrier Mobilities and Lifetimes in Organolead Trihalide Perovskites. *Adv. Mater.* **2014,** *26* (10), 1584-1589.
7. Ponseca, C. S.; Savenije, T. J.; Abdellah, M.; Zheng, K. B.; Yartsev, A.; Pascher, T.; Harlang, T.; Chabera, P.; Pullerits, T.; Stepanov, A.; Wolf, J. P.; Sundstrom, V., Organometal

Halide Perovskite Solar Cell Materials Rationalized: Ultrafast Charge Generation, High and Microsecond-Long Balanced Mobilities, and Slow Recombination. *J. Am. Chem. Soc.* **2014,** *136* (14), 5189-5192.
8. Protesescu, L.; Yakunin, S.; Bodnarchuk, M. I.; Krieg, F.; Caputo, R.; Hendon, C. H.; Yang, R. X.; Walsh, A.; Kovalenko, M. V., Nanocrystals of Cesium Lead Halide Perovskites ($CsPbX_3$, X = Cl, Br, and I): Novel Optoelectronic Materials Showing Bright Emission with Wide Color Gamut. *Nano Lett.* **2015,** *15* (6), 3692-3696.
9. Yantara, N.; Bhaumik, S.; Yan, F.; Sabba, D.; Dewi, H. A.; Mathews, N.; Boix, P. P.; Demir, H. V.; Mhaisalkar, S., Inorganic Halide Perovskites for Efficient Light-Emitting Diodes. *J. Phys. Chem. Lett.* **2015,** *6* (21), 4360-4364.
10. Li, X.; Wu, Y.; Zhang, S.; Cai, B.; Gu, Y.; Song, J.; Zeng, H., $CsPbX_3$ Quantum Dots for Lighting and Displays: Room-Temperature Synthesis, Photoluminescence Superiorities, Underlying Origins and White Light-Emitting Diodes. *Adv. Funct. Mater.* **2016,** *26* (15), 2435-2445.
11. Li, G.; Rivarola, F. W. R.; Davis, N. J. L. K.; Bai, S.; Jellicoe, T. C.; de la Peña, F.; Hou, S.; Ducati, C.; Gao, F.; Friend, R. H.; Greenham, N. C.; Tan, Z.-K., Highly Efficient Perovskite Nanocrystal Light-Emitting Diodes Enabled by a Universal Crosslinking Method. *Adv. Mater.* **2016,** *28* (18), 3528-3534.
12. Wang, Q.; Shao, Y.; Xie, H.; Lyu, L.; Liu, X.; Gao, Y.; Huang, J., Qualifying composition dependent p and n self-doping in $CH_3NH_3PbI_3$. *Appl. Phys. Lett.* **2014,** *105* (16), 163508.
13. Song, D.; Cui, P.; Wang, T.; Wei, D.; Li, M.; Cao, F.; Yue, X.; Fu, P.; Li, Y.; He, Y.; Jiang, B.; Trevor, M., Managing Carrier Lifetime and Doping Property of Lead Halide Perovskite by Postannealing Processes for Highly Efficient Perovskite Solar Cells. *J. Phys. Chem. C* **2015,** *119* (40), 22812-22819.
14. Abdelhady, A. L.; Saidaminov, M. I.; Murali, B.; Adinolfi, V.; Voznyy, O.; Katsiev, K.; Alarousu, E.; Comin, R.; Dursun, I.; Sinatra, L.; Sargent, E. H.; Mohammed, O. F.; Bakr, O. M., Heterovalent Dopant Incorporation for Bandgap and Type Engineering of Perovskite Crystals. *J. Phys. Chem. Lett.* **2016,** *7* (2), 295-301.
15. Zhang, J.; Shang, M. H.; Wang, P.; Huang, X. K.; Xu, J.; Hu, Z. Y.; Zhu, Y. J.; Han, L. Y., n-Type Doping and Energy States Tuning in $CH_3NH_3Pb_{1-x}Sb_{2x/3}I_3$ Perovskite Solar Cells. *ACS Energy Lett.* **2016,** *1* (3), 535-541.
16. Wang, J. T.-W.; Wang, Z.; Pathak, S.; Zhang, W.; deQuilettes, D. W.; Wisnivesky-Rocca-Rivarola, F.; Huang, J.; Nayak, P. K.; Patel, J. B.; Mohd Yusof, H. A.; Vaynzof, Y.; Zhu, R.; Ramirez, I.; Zhang, J.; Ducati, C.; Grovenor, C.; Johnston, M. B.; Ginger, D. S.; Nicholas, R. J.; Snaith, H. J., Efficient perovskite solar cells by metal ion doping. *Energy Environ. Sci.* **2016,** *9* (9), 2892-2901.
17. Zhou, Y.; Yong, Z.-J.; Zhang, K.-C.; Liu, B.-M.; Wang, Z.-W.; Hou, J.-S.; Fang, Y.-Z.; Zhou, Y.; Sun, H.-T.; Song, B., Ultrabroad Photoluminescence and Electroluminescence at New Wavelengths from Doped Organometal Halide Perovskites. *J. Phys. Chem. Lett.* **2016,** *7* (14), 2735-2741.
18. Jiang, Q. L.; Chen, M. M.; Li, J. Q.; Wang, M. C.; Zeng, X. Q.; Besara, T.; Lu, J.; Xin, Y.; Shan, X.; Pan, B. C.; Wang, C. C.; Lin, S. C.; Siegrist, T.; Xiao, Q. F.; Yu, Z. B., Electrochemical Doping of Halide Perovskites with Ion Intercalation. *ACS Nano* **2017,** *11* (1), 1073-1079.

19. Jiang, Q.; Zeng, X.; Wang, N.; Xiao, Z.; Guo, Z.; Lu, J., Electrochemical Lithium Doping Induced Property Changes In Halide Perovskite CsPbBr3 Crystal. *ACS Energy Lett.* **2018,** *3* (1), 264-269.
20. Dawson, J. A.; Naylor, A. J.; Eames, C.; Roberts, M.; Zhang, W.; Snaith, H. J.; Bruce, P. G.; Islam, M. S., Mechanisms of Lithium Intercalation and Conversion Processes in Organic-Inorganic Halide Perovskites. *ACS Energy Lett.* **2017,** *2* (8), 1818-1824.
21. Vicente, N.; Garcia-Belmonte, G., Methylammonium Lead Bromide Perovskite Battery Anodes Reversibly Host High Li-Ion Concentrations. *J. Phys. Chem. Lett.* **2017,** *8* (7), 1371-1374.
22. Mulder, J. T.; du Fosse, I.; Jazi, M. A.; Manna, L.; Houtepen, A. J., Electrochemical p-Doping of $CsPbBr_3$ Perovskite Nanocrystals. *ACS Energy Lett.* **2021,** *6* (7), 2519-2525.
23. Hasan, M.; Venkatesan, S.; Lyashenko, D.; Slinker, J. D.; Zakhidov, A., Solvent Toolkit for Electrochemical Characterization of Hybrid Perovskite Films. *Anal. Chem.* **2017,** *89* (18), 9649-9653.
24. Samu, G. F.; Scheidt, R. A.; Kamat, P. V.; Janáky, C., Electrochemistry and Spectroelectrochemistry of Lead Halide Perovskite Films: Materials Science Aspects and Boundary Conditions. *Chem. Mat.* **2018,** *30* (3), 561-569.
25. Zakhidov, A. A.; Lee, J.-K.; Fong, H. H.; DeFranco, J. A.; Chatzichristidi, M.; Taylor, P. G.; Ober, C. K.; Malliaras, G. G., Hydrofluoroethers as Orthogonal Solvents for the Chemical Processing of Organic Electronic Materials. *Adv. Mater.* **2008,** *20* (18), 3481-3484.
26. Zakhidov, A. A.; Reineke, S.; Lüssem, B.; Leo, K., Hydrofluoroethers as heat-transfer fluids for OLEDs: Operational range, stability, and efficiency improvement. *Org. Electron.* **2012,** *13* (3), 356-360.
27. Krotkus, S.; Nehm, F.; Janneck, R.; Kalkura, S.; Zakhidov, A.; Schober, M.; Hild, O.; Kasemann, D.; Hofmann, S.; Leo, K.; Reineke, S., *Influence of bilayer resist processing on p-i-n OLEDs: towards multicolor photolithographic structuring of organic displays*. SPIE: 2015; Vol. 9360.
28. Venkatesan, S.; Hasan, M.; Kim, J.; Rady, N. R.; Sohal, S.; Neier, E.; Yao, Y.; Zakhidov, A., Tailoring nucleation and grain growth by changing the precursor phase ratio for efficient organic lead halide perovskite optoelectronic devices. *J. Mater. Chem. C* **2017,** *5* (39), 10114-10121.
29. Masi, S.; Gualdrón-Reyes, A. F.; Mora-Seró, I., Stabilization of Black Perovskite Phase in $FAPbI_3$ and $CsPbI_3$. *ACS Energy Lett.* **2020,** *5* (6), 1974-1985.
30. Adinolfi, V.; Yuan, M.; Comin, R.; Thibau, E. S.; Shi, D.; Saidaminov, M. I.; Kanjanaboos, P.; Kopilovic, D.; Hoogland, S.; Lu, Z.-H.; Bakr, O. M.; Sargent, E. H., The In-Gap Electronic State Spectrum of Methylammonium Lead Iodide Single-Crystal Perovskites. *Adv. Mater.* **2016,** *28* (17), 3406-3410.
31. Zhou, X.; Li, X.; Liu, Y.; Huang, F.; Zhong, D., Interface electronic properties of co-evaporated $MAPbI_3$ on ZnO(0001): In situ X-ray photoelectron spectroscopy and ultraviolet photoelectron spectroscopy study. *Appl. Phys. Lett.* **2016,** *108* (12), 121601.
32. Jung, H. S.; Park, N.-G., Perovskite Solar Cells: From Materials to Devices. *Small* **2015,** *11* (1), 10-25.
33. Alahbakhshi, M.; Mishra, A.; Haroldson, R.; Ishteev, A.; Moon, J.; Gu, Q.; Slinker, J. D.; Zakhidov, A. A., Bright and Effectual Perovskite Light-Emitting Electrochemical Cells Leveraging Ionic Additives. *ACS Energy Lett.* **2019,** *4*, 2922-2928.